Inorganic Chemistry

Article

pubs.acs.org/IC

Spirobifluorene Bridged Ir(III) and Os(II) Polypyridyl Arrays: Synthesis, Photophysical Characterization, and Energy Transfer Dynamics

Barbara Ventura,*[,†] Andrea Barbieri,[†] Alessandra Degli Esposti,[†] Julie Batcha Seneclauze,[‡] and Raymond Ziessel*[,‡]

[†]Istituto per la Sintesi Organica e la Fotoreattività, Consiglio Nazionale delle Ricerche (ISOF-CNR), Via P. Gobetti 101, 40129 Bologna, Italy

[‡]Laboratoire de Chimie Organique et Spectroscopies Avancées (LCOSA) associé au CNRS (UMR 7515) École, de Chimie, Polymères, Matériaux (ECPM), Université de Strasbourg (UdS), 25 rue Becquerel, 67087 Strasbourg Cedex 02, France

Supporting Information

ABSTRACT: The synthesis, characterization, photophysics, and time-dependent density functional theory (TD-DFT) calculations of spirobifluorene-bipyridine based iridium(III), osmium(II), and mixed Ir/Os complexes are presented. The preparation of the reference and mixed complexes proceeded step-by-step and microwave irradiation facilitated the complexation of osmium. The absorption of the target heterobimetallic derivative, **Ir-L-Os**, is described by linear combination of half of the absorption spectra of the homobimetallic analogues, **Ir-L-Ir** and **Os-L-Os**, due to the occurrence of mixed ligand and metal based transitions when the spirobifluorene-$(bpy)_2$ bridging ligand **L** is linked to the metal, confirming a negligible interaction between the substituted metallic chromophores. TD-DFT calculations on monometallic, homo- and hetero-bimetallic complexes fully disentangled the origin of the absorption features. Noticeably, in the mixed **Ir-L-Os** complex an almost quantitative energy transfer from the ^{3}Ir to the ^{3}Os MLCT state is occurring, with a rate constant of 4.1×10^8 s^{-1} and nearly exclusively via a Dexter-type mechanism mediated by the orbitals of the spiroconjugated ligand. This result, together with the outcomes of the TD-DFT calculations, supports the existence of spiroconjugation and evidences the interesting role of this kind of bridge in the energy transfer dynamics of the arrays. In all the complexes, moreover, the ligand fluorescence is heavily quenched by energy transfer processes toward the metallic appended units; the rate constant is estimated in the order of 10^{10} s^{-1} for **Ir-L-Os** and higher than 10^{12} s^{-1} for the other complexes. In the heterometallic array, both at room temperature and at 77 K, all photons are thus funneled to the emissive Os ^{3}MLCT state, which acts as energy trap for the antenna cascade.

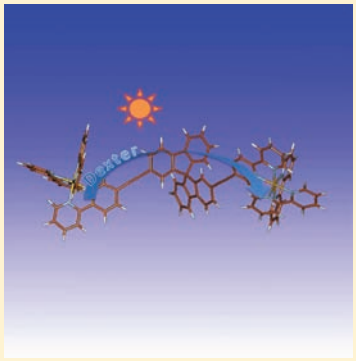

INTRODUCTION

The design and synthesis of new supramolecular architectures for light collection and conversion with a well-defined spatial arrangement of the photoactive units is a challenging task that finds great interest in photonic and optoelectronic applications.[1−8]

The main topic is the development of synthetic procedures for the construction of multichromophoric architectures where a central molecular motif can be functionalized in specific positions with light-harvesting chromophores. The skeleton structure and the appended chromophores need to be chosen according to their topology and photophysical properties, respectively, to ensure energy and spatially driven light-harvesting processes. Moreover, it might be considered that, when the central scaffold is not only an "innocent" suitable structural motif but is itself a photoactive component, it can participate in the light-harvesting process making the supramolecular system a very effective antenna, with promising applications in solar conversion and lighting devices. Recently, some examples of dendrimeric multichromophoric arrays based on a central truxene platform and appended transition metal complexes or organic chromophores showed the occurrence of fast energy-transfer steps from all the components toward a specifically designed collector unit.[9−11]

The design of arrays where an orthogonal orientation of the chromophoric units in space is combined with a nonzero photophysical contribution of the core scaffold is appealing. This can be achieved only exploiting the particular properties of the so-called "spiroconjugation", where two π systems are held in perpendicular planes by a common carbon atom of tetrahedral geometry, with a significant electron delocalization over the carbon atoms adjacent to the central one.[12−16] Following this concept the spirobifluorene unit can be considered as a promising building material for newly conceived supramolecular arrays. The 2,2′-functionalization of 9,9′-spirobifluorene, in fact, allowed obtaining orthogonally arranged structures with favorable linear and nonlinear optical

Received: August 31, 2011
Published: February 22, 2012

dx.doi.org/10.1021/ic201903g | Inorg. Chem. 2012, 51, 2832−2840

properties,[17−19] reinforcing the evidence of the particular conjugation provided by this type of bridge. Spirobifluorene is then itself an interesting photoactive module, since it is a very efficient blue emitter, largely employed in the synthesis of blue-emitting conjugated polymers for polymer-based light-emitting devices (POLEDs), two-photon absorption, and organic optoelectronics.[20−25] Recently it has been shown that the rigid spiroconfiguration confers to the spiro-based organic dyes the property of avoiding aggregation and consequently self-quenching when applied in DSSCs.[26] Moreover, it increases the rigidity of the dyes with an enhancement of the emission quantum yield, useful for biological labeling applications.[27]

We report here on the synthesis and photophysical characterization of a newly designed series of arrays where Ir(III) and Os(II) polypyridyl complexes have been linked to the 2,2′-positions of a spirobifluorene scaffold via ethynylenic linkages. This work follows recent interest of the authors on the synthesis and photophysical characterization of supramolecular arrays containing transition metal complexes and organic scaffolds, with particular attention on the role of the bridge in the photophysics of the arrays.[10,11] The present series consists of the heterometallic triad **Ir-L-Os**, the homometallic dyads **Ir-L-Ir** and **Os-L-Os**, and model complexes **Ir-L** and **Os-L** (Chart 1). The bipyridyl substituted spirobifluorene ligand **L** has been also characterized for comparison purposes. The optical properties of the complexes have been analyzed by means of steady-state and time-resolved spectroscopy and the absorption features have been assigned by means of time-dependent density functional theory (TD-DFT) studies. Energy transfer dynamics in triad **Ir-L-Os** has been analyzed by comparison with the properties of the reference monometallic and homo bimetallic complexes.

Chart 1. Schematic Structure of the Investigated Compounds (The Charges Have Been Omitted for Clarity)

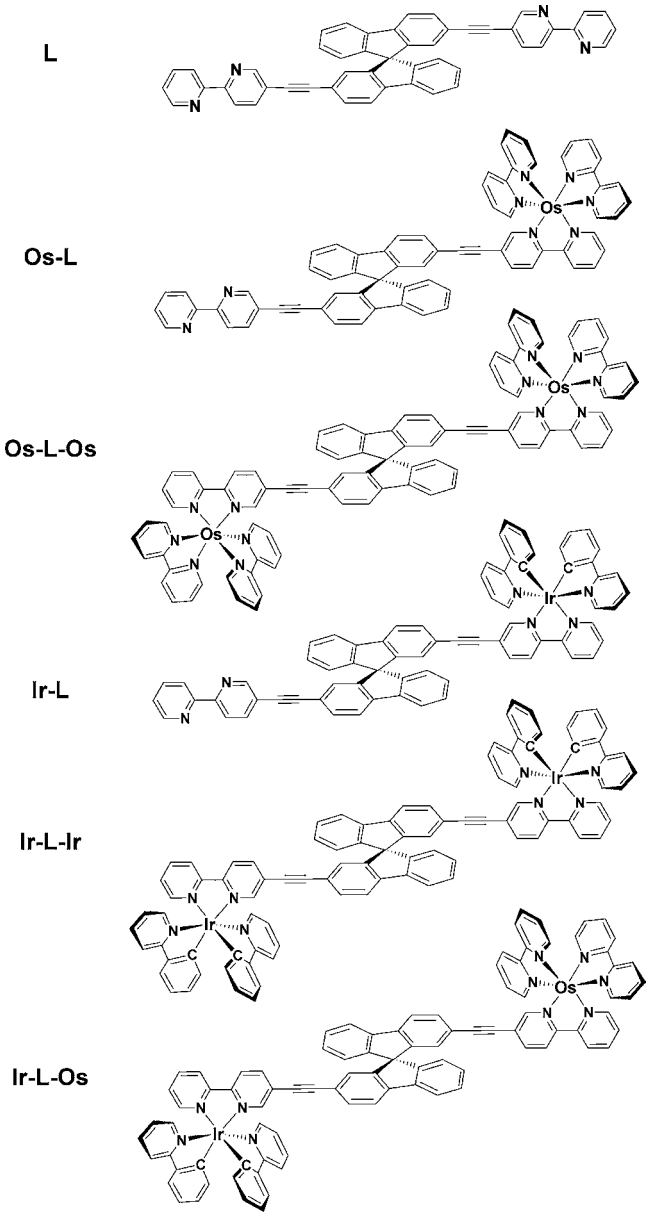

EXPERIMENTAL SECTION

Synthesis and Characterization. *Preparation of Ligand L.* 2,2′-Bis(trifluoromethylsulfoxy)-9,9′-spirobifluorene (1.000 g, 1.63 mmol) and 5-ethynyl-2,2′-bipyridine (1.098 g, 8.15 mmol) were dissolved in *n*-propylamine (50 mL). Argon was bubbled through the mixture for 30 min; $[Pd(PPh_3)_4]$ (336 mg, 0.30 mmol) was added and the stirred mixture was heated at 50 °C for 18 h. After rotary evaporation of the solvent, the residue was extracted with dichloromethane and washed with water and saturated brine. The organic layer was filtered over hygroscopic cotton wool and evaporated. The ligand was purified by column chromatography on aluminum oxide and eluted with dichloromethane−petroleum ether (v/v: 5/1 to 1/0) affording 648 mg (83%) of 2,2′-bis(2,2′-bipyridine-5-ethynyl)-9,9′-spirobifluorene **L**. ^{1}H NMR ($CDCl_3$, 300 MHz): δ 8.70 (m, 4H), 8.41 (d, 4H, ^4J = 7.5 Hz), 7.90−7.82 (m, 8H), 7.61 (d, 2H, ^3J = 7.8 Hz), 7.42 (t, 2H, ^3J = 8.2 Hz), 7.32−7.26 (m, 2H), 7.17 (t, 2H, ^3J = 8.2 Hz), 6.97 (s, 2H), 6.79 (d, 2H, ^3J = 7.5 Hz). ^{13}C NMR ($CDCl_3$, 50 MHz): δ 155.5, 154.7, 151.5, 149.25, 148.5, 148.4, 142.5, 141.0, 139.2, 136.9, 131.8, 128.6, 128.2, 127.4, 124.2, 123.9, 121.9, 121.3, 120.5, 120.3, 120.2, 93.8, 86.8, 65.6. EIMS *m/e* (nature of the peak, relative intensity) 673.2 ($[M + H]^+$, 100). Anal. Calcd. for $C_{49}H_{28}N_4$: C, 87.48; H, 4.19; N, 8.33; found: C, 87.22; H, 3.92; N, 8.17.

General Procedure for the Counterion Metathesis. After the complexation reaction was completed and the reaction mixture evaporated to dryness, the residue was dissolved in the minimum of DMF and dropwise added to a vigorously stirred aqueous solution of KPF_6 (200 mg in 10 mL). The resulting precipitate was either filtered off and washed with water or extracted with dichloromethane and the organic layer washed with water and then rotary evaporated.

Preparation of the Os-L and Os-L-Os Complexes. Ligand **L** (29 mg, 43 μmol), and $[Os(bpy)_2Cl_2]$ (34 mg, 47 μmol) were suspended in EtOH (10−20 mL) in a Teflon reactor. The mixture was irradiated with microwaves of 1200 W at 180 °C for 30 min. The solvent was evaporated and the counterion was exchanged according to the general procedure. After washing with water, the complexes were separated by column chromatography on aluminum oxide eluting with dichloromethane−methyl alcohol (v/v: 100/0 to 94/6) to afford 24 mg (37%) of **Os-L** and 20 mg (21%) of **Os-L-Os** as black crystals after recrystallization from dichloromethane−diethyl ether.

Os-L. ^{1}H NMR (d_6-acetone, 300 MHz): δ 8.79−8.68 (m, 8H), 8.48−8.43 (m, 2H), 8.14−7.87 (m, 18 H), 7.70 (m, 1H), 7.55−7.38 (m, 9H), 7.28−7.21 (m, 2H), 6.89 (s, 1H), 6.78−6.73 (m, 2H) 6.79 (s, 1H). ESI-MS *m/z* (nature of the peak, relative intensity) 1321.2 ($[M - PF_6]^+$, 100), 588.2 ($[M - 2PF_6]^{2+}$, 30). Anal. Calcd. for $C_{69}H_{44}F_{12}N_8OsP_2$: C, 56.56; H, 3.03; N, 7.65; found: C, 56.28; H, 2.92; N, 7.41.

Os-L-Os. ^{1}H NMR (d_6-acetone, 300 MHz): δ 8.78−8.69 (m, 12H), 8.10−7.87 (m, 28H), 7.55−7.40 (m, 14H), 7.26 (m, 2H), 6.72 (d, 2H, ^3J = 7.7 Hz), 6.65 (d, 2H, ^3J = 2.7 Hz). ESI-MS *m/z* (nature of the peak, relative intensity) 2112.2 ($[M - PF_6]^+$, 65), 985.1 ($[M - 2PF_6]^{2+}$, 100), 608.3 ($[M - 3PF_6]^{3+}$, 15). Anal. Calcd. for

dx.doi.org/10.1021/ic201903g | Inorg. Chem. 2012, 51, 2832−2840

Scheme 1. Synthesis of the Ditopic Ligand and Osmium Complexes

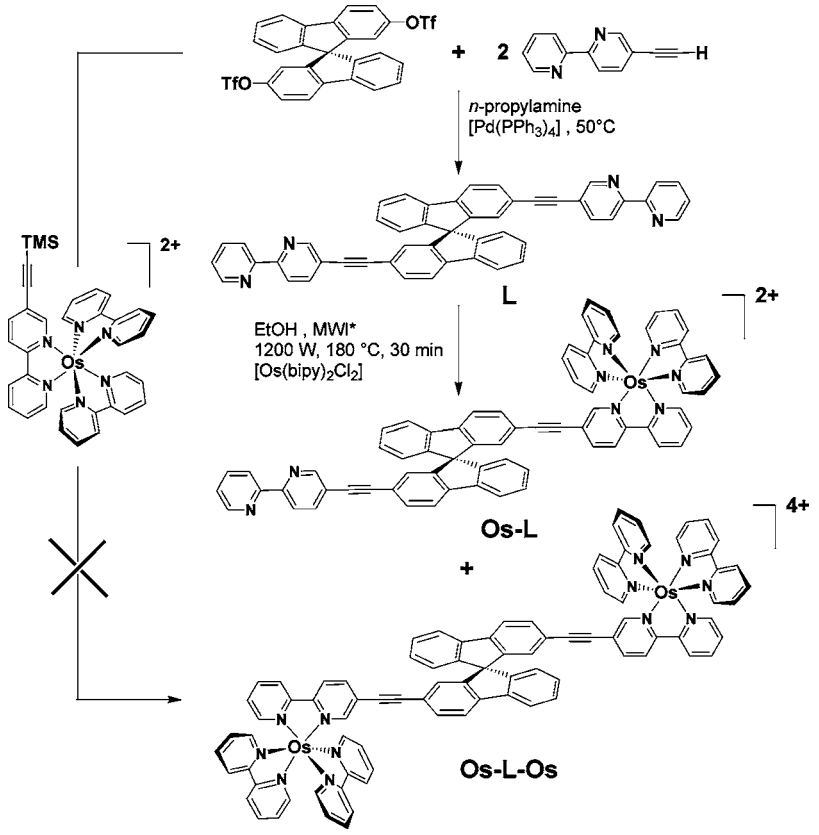

$C_{89}H_{60}F_{24}N_{12}Os_2P_4$: C, 47.34; H, 2.68; N, 7.44; found: C, 47.09; H, 2.62; N, 7.17.

Preparation of the Ir-L and Ir-L-Ir Complexes. Ligand **L** (50 mg, 30 μmol) was dissolved in mixture of dichloromethane and methanol (2 mL). The dimer $[(C\hat{}N)_2IrCl]_2$ (29 mg, 27 μmol) was added and the mixture was heated for 18 h at 60 °C. The solvent was then rotary evaporated and the residue was washed with water. The counterion was exchanged according to the general procedure and the complexes were separated by column chromatography on aluminum oxide with a mixture of dichloromethane−methyl alcohol (v/v: 100/0 to 98/2) to afford 38 mg (39%) of **Ir-L** and 30 mg (21%) of **Ir-L-Ir** as yellow powder after recrystallization from dichloromethane−pentane.

Ir-L. ^{1}H NMR (acetone d^6, 300 MHz): δ 8.83 (t, 2H, ^3J = 6.8 Hz), 8.73 (s, 1H), 8.68 (d, 1H, ^3J = 4.5 Hz), 8.46 (dd, 2H, ^4J = 3.0 Hz, ^3J = 8.3 Hz), 8.31−8.04 (m, 9H), 8.00−7.87 (m, 6H), 7.83−7.78 (m, 2H), 7.74−7.67 (m, 4H), 7.57−7.48 (m, 3H), 7.43 (t, 1H, ^3J = 7.1 Hz), 7.30−7.25 (m, 2H), 7.12 (q, 2H, ^3J = 6.4 Hz), 7.06−6.77 (m, 8H), 6.30 (d, 2H, ^3J = 7.5 Hz). ESI-MS *m/z* (nature of the peak, relative intensity) 1173.2 ($[M - PF_6]^+$, 100). Anal. Calcd. for $C_{71}H_{44}F_6IrN_6P$: C, 64.68; H, 3.36; N, 6.37; found: C, 64.42; H, 3.16; N, 6.18.

Ir-L-Ir. ^{1}H NMR (acetone d^6, 300 MHz): δ 8.8 (d, 4H, ^3J = 8.3 Hz), 8.32−7.69 (m, 28H), 7.59−7.48 (m, 4H), 7.27 (m, 2H), 7.17−7.02 (m, 6H), 6.93−6.66 (m, 12H), 6.30 (m, 4H). ESI-MS *m/z* (nature of the peak, relative intensity) 1818.2 ($[M - PF_6]^+$, 50), 837.2 ($[M - 2PF_6]^+$, 100). Anal. Calcd. for $C_{93}H_{60}F_{12}Ir_2N_8P_2$; C, 56.88; H, 3.08; N, 5.71; found: C, 56.62; H, 2.94; N, 5.45.

Preparation of the Ir-L-Os Complex. The **Os-L** complex (20 mg, 14 μmol) and $[(C\hat{}N)_2IrCl]2$ complex (8 mg, 7 μmol) were dissolved in dichloromethane/methanol (2 mL/8 mL) and the solution was heated for 18 h at 60 °C. The solvent was then evaporated to dryness, the residue was washed with water, and anion exchange ensured using the general procedure. The resulting complex was purified by column chromatography on aluminum oxide eluting with dichloromethane−methyl alcohol (v/v: 100/0 to 94/6) to afford 22 mg (29%) of **Ir-L-Os** as dark crystals after recrystallization from dichloromethane−pentane. ^{1}H NMR (acetone d^6, 300 MHz): δ 8.83−8.77 (m, 8H), 8.29−8.18 (m, 4H), 8.16−7.89 (m, 20H), 7.82−7.78 (m, 2H), 7.72−7.72 (m, 2H), 7.56−7.45 (m, 8H), 7.28−7.23 (m, 2H), 7.14−7.10 (m, 2H), 7.04−6.94 (m, 2H), 6.93−6.66 (m,8H), 6.30 (m, 2H). ESI-MS *m/z* (nature of the peak, relative intensity) 1967.4 ($[M - PF_6]^+$, 100), 829.5. Anal. Calcd. for $C_{91}H_{60}F_{18}IrN_{10}OsP_3$: C, 51.78; H, 2.87; N, 6.64; found: C, 51.96; H, 3.02; N, 6.99.

Photophysical Measurements. Spectroscopic-grade solvents (C. Erba) were used as received. The absorption spectra were recorded for dilute solutions (10^{-6} M) on a Perkin-Elmer Lambda 950 UV/vis/NIR spectrophotometer in 1-cm path length optical Suprasil Quartz (QS) cuvettes. Emission spectra in the UV−vis range were measured in right angle mode using a Spex Fluorolog II spectrofluorimeter, equipped with a Hamamatsu R928 phototube. Luminescence in the NIR was examined by a FLS920 spectrofluorimeter (Edinburgh) equipped with an Hamamatsu R5509-72 supercooled photomultiplier tube at 193 K and a TM300 emission monochromator with a grating blazed at 1000 nm. Corrected spectra were employed throughout this work by applying to the raw data a correction curve for the wavelength-dependent phototubes response. Air-free samples were obtained by bubbling the solutions for 10 min with a stream of argon in home-modified 1-cm fluorescence cuvettes. Luminescence quantum yields (ϕ_{em}) were evaluated from the area of the corrected luminescence spectra, with reference to quinine sulfate in air-equilibrated 1 N H_2SO_4 (ϕ_r = 0.546)[28] for the ligand, to $[Ru(bpy)_3]Cl_2$ in air-equilibrated water (ϕ_r = 0.028)[28] for the Ir-based emission, and to $[Os(ttpy)_2]^{2+}$ (ϕ_r = 0.021, O_2-freebutyronitrile, ttpy is tolylterpyridine)[29] for the Os-based emission, by using the following equation:[30]

$$\phi_{em} = \frac{A_r n^2 I}{n_r^2 I_r A}\phi_r$$

where *A* and *n* are the absorbance values at the employed excitation wavelength and refractive index of the solvent, respectively, and *I* is the integrated emission intensity (subscript r is for reference). The

dx.doi.org/10.1021/ic201903g | Inorg. Chem. 2012, 51, 2832−2840

concentration of the sample solutions was adjusted to obtain absorption values $A < 0.1$ at the excitation wavelength. Estimated uncertainties on band maxima and luminescence intensities are 2 nm and 20%, respectively.

The intramolecular rate constant for a general energy-transfer process can be obtained from the following equation:[31,32]

$$k_{EnT} = \frac{1}{\tau} - \frac{1}{\tau_0}$$

in which τ is the lifetime of the donor quenched emission and τ_0 is the donor unquenched lifetime.

The efficiency of the intramolecular energy-transfer process can be evaluated by using the equation

$$\eta_{EnT} = k_{EnT}/(k_{EnT} + k_{in})$$

in which $k_{in} = 1/\tau_0$ is the intrinsic deactivation rate constant of the unquenched donor, and k_{EnT} has been defined before.

Experiments at 77 K in MeOH/EtOH (1:4) frozen glasses made use of quartz capillary tubes immersed in liquid nitrogen contained in a homemade quartz dewar. Excitation spectra, both at room temperature and at 77 K, were obtained at the different luminescence peaks by using the Spex Fluorolog II spectrofluorimeter.

Luminescence lifetimes in the ns–μs range were measured with an IBH 5000F time-correlated single-photon counting device, by using pulsed NanoLED excitation sources at 331, 375, and 465 nm (pulse width $\leq$ 0.6 ns) for excitation of the ligand, of the Ir-center, and of the Os-center of the arrays, respectively. Analysis of the luminescence decay profiles against time was accomplished with the DAS6 Decay Analysis Software provided by the manufacturer. The phosphorescence spectrum and lifetime of the free ligand were measured at 77 K on the same IBH 5000F time-correlated single-photon counting device by using a pulsed SpectraLED excitation source at 370 nm, and performing a time-resolved emission spectra (TRES) procedure. The spectrum was obtained upon selection of slices in a linearity region of the decays on a semilog scale at the different emission wavelengths. The lifetime analysis was performed on the whole series of decays with the Global Analysis Module of the DAS6 Decay Analysis Software provided by the manufacturer. The solution was prepared in 3 mL of MeOH/EtOH (1:4) with the addition of one drop of CH_3I to induce phosphorescence by means of external heavy atom effect. Experimental uncertainties in the lifetime determinations are estimated to be 10%.

All the examined compounds were found to be thermally and photochemically stable in solution.

Theoretical Calculations. The electronic properties of Os(II) and Ir(III) complexes were investigated by means of Density Functional Theory (DFT)[33,34] and Time Dependent DFT (TD-DFT)[35−37] methods implemented in the Gaussian 09 software package[38] using the hybrid meta exchange-correlation functional M06.[39] Small-core relativistic ECPs and correlation consistent basis set of double-zeta quality were employed for Os and Ir[40] with 6-31G* basis set[41,42] for all the other atoms. Solvation was accounted for by means of the polarizable continuum model (PCM)[43] with the default formalism. The spiroconjugation was investigated by means of the natural bond population analysis (NBO version 3.1)[44] by considering the strengths of the donor–acceptor interactions. Details on the calculations, along with the electron density plots and the calculated transitions of the examined complexes are included within the Supporting Information.

RESULTS AND DISCUSSION

Synthesis. The ditopic ligand **L** was prepared in a single step from slight excess of 5-ethynyl-2,2′-bipyridine[45] and a racemic mixture of 2,2′-bis(trifluoromethylsulfoxy)-9,9′-spirobifluorene.[46] The double cross-coupling reaction is promoted by a Pd(0) catalyst precursor which facilitates the one-pot synthesis of **L** (Scheme 1). With this ligand in hand it was convenient to complex the bipyridine subunits with either one or two osmium centers under microwave irradiation. This statistical complexation provides 37% of **Os-L** and 21% of **Os-L-Os** without degradation of the ligand which could be easily recovered by column chromatography and recycled (40% recovering of **L**). Increasing the equivalent of $[Os(bpy)_2Cl_2]$[47] does increase the yield of the dinuclear complex to 43%, but degrades the ligand, which could not be recovered. An alternative protocol using a preformed osmium complex carrying a trimethylsilyl-alkyne function and in situ deprotection and cross-coupling failed leading to intractable mixtures of complex from which homocoupled bis Os complexes could be isolated.

Preparation of the mono- and bis-iridium complexes used a standard protocol of heating the ligand with the $[Ir(C\hat{}N)_2Cl]_2$[48] precursor (Scheme 2). Routinely, 39% of **Ir-L**

Scheme 2. Synthesis of the Iridium and Mixed Iridium–Osmium Complexes

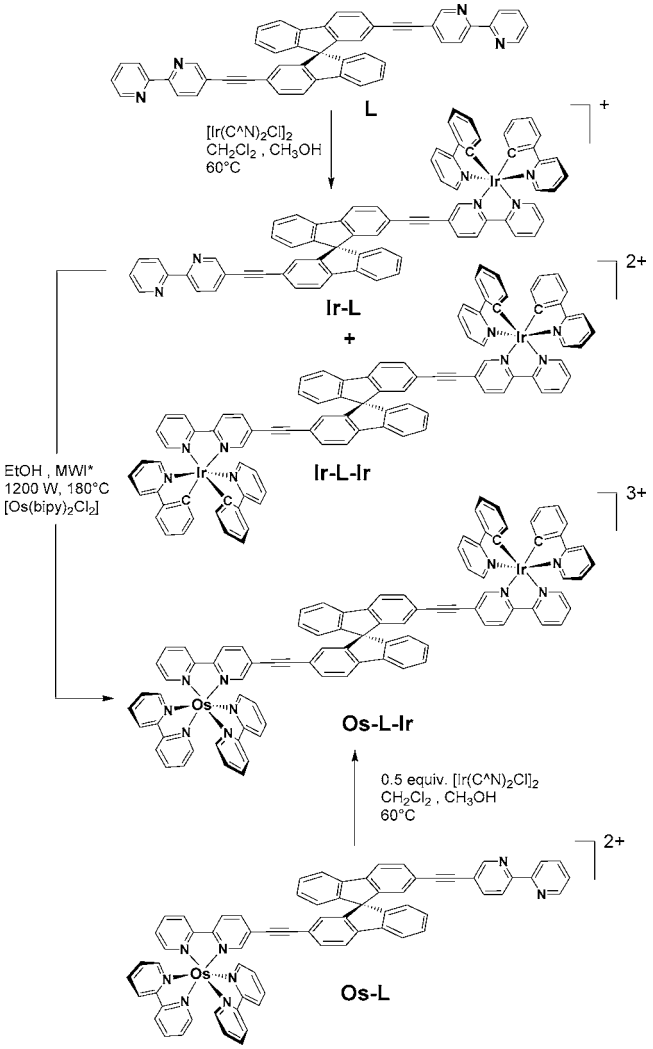

and 21% of **Ir-L-Ir** were easily obtained and column chromatography allowed recovery of 40% of the unreacted ligand **L**. Increasing the stoichiometry of the Ir-precursor to 2 to 1 (dimer versus **L**) increases the yield of the dinuclear complex to 83%. No degradation of the ligand was observed in this case. Interestingly, the mixed heterodinuclear complex **Os-L-Ir** could be prepared either from the mono-Ir or mono-Os complex (Scheme 2). We preferred the latter route due to the

dx.doi.org/10.1021/ic201903g | Inorg. Chem. 2012, 51, 2832–2840

better preparative yield and to the ease of purification of the resulting **Os-L-Ir** complex by column chromatography. The large difference in polarity among the ligand, mono-, and dinuclear complexes (Figure S1), and their good solubility allow facile purification by column chromatography using alumina as fixed phase and dichloromethane/methanol mixtures as mobile phase. Furthermore, all the complexes were carefully recrystallized in adequate solvent (see Experimental Section for details) to prevent any residual impurities. All these novel complexes were unambiguously characterized by NMR and ESI spectroscopy and elemental analysis and all data confirm the molecular structures drawn in Chart 1.

The purity of the ligand and complexes has been checked by proton NMR and thin-layer-chromatography (TLC, Figure S1). Both techniques clearly exclude the noticeable presence of residual free ligand (estimated <0.1%) in the mentioned complexes. In particular, TLC experiments carried out under different elution conditions are representative of the global charge of the complexes and clearly state in favor of the absence of noticeable amounts of free ligand and was also confirmed by broad band excitation at 365 nm with a bench lamp. Furthermore, the ^{1}H NMR of the ligand **L** exhibits two diagnostic signals at 8.41 and 7.61 ppm. For the mononuclear complexes **Os-L** and **Ir-L** the signal at 7.61 ppm is not observed, whereas for the dinuclear **Os-L-Os**, **Ir-L-Ir**, and **Ir-L-Os** complexes both resonances at 8.41 and 7.61 ppm are absent from the spectra (Figures S2−S7). These ^{1}H NMR spectra were repeated after 48 h on the same samples kept in the solution without particular protection against daylight.

Absorption. The main absorption data for the examined compounds are summarized in Table 1. Figure 1 compares the absorption spectra of ligand **L** and monometallic complexes **Ir-L** and **Os-L**, whereas Figure 2 reports the absorption spectra of **Ir-L-Ir**, **Os-L-Os**, and **Ir-L-Os** (with the spectrum of **L** shown again for comparison purposes).

Table 1. Absorption Properties of Ligand and Complexes[a]

	λ_{max} (nm)	ε (M^{-1} cm^{-1})
L	343	88,900
	361	78,300
Ir-L	297	72,900
	341	83,000
	358	84,000
	383 (sh)	38,700
Ir-L-Ir	291	87,400
	366	74,500
Os-L	291	102,400
	340	77,900
	358	78,500
	383 (sh)	39,900
	450	11,700
	600	3,100
Os-L-Os	291	150,600
	370	77,000
	453	21,100
	600	5,700
Ir-L-Os	291	119,500
	361	71,400
	450	12,300
	600	3,200

[a] In CH_2Cl_2 for the ligand and in CH_3CN for the complexes, at 298 K.

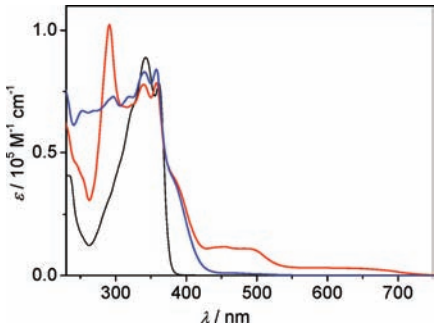

Figure 1. Absorption spectra of CH_3CN solutions of **Ir-L** (blue), **Os-L** (red), and a CH_2Cl_2 solution of **L** (black).

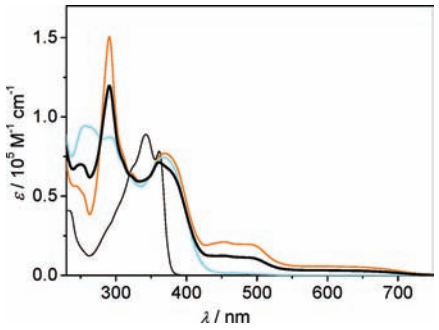

Figure 2. Absorption spectra of CH_3CN solutions of **Ir-L-Ir** (cyan), **Os-L-Os** (orange), **Ir-L-Os** (black thick), and a CH_2Cl_2 solution of **L** (black thin).

The absorption spectrum of ligand **L**, with maxima at 343 and 361 nm, is red-shifted with respect to bare spirobifluorene, whose absorption extends only up to 320 nm.[19] The bathochromic shift is ascribed to the conjugation introduced by the two ethynyl-bipyridine terminals. The spectra of the complexes **Ir-L** and **Os-L** display the two characteristic peaks of ligand **L**, together with features, for wavelengths higher than 370 nm, usually ascribed to MLCT transitions of the $Ir(ppy)_3$ or $Os(bpy)_3$ type moieties, respectively (Figure 1).[49,50] The spectral features of the three bimetallic arrays are less trivial: here the peaks of the ligand are no more discernible whereas a clear new band that peaks at 371 nm appears, related to the metal coordination of both bpy terminals of the aromatic bridging ligand. The absorption spectrum of triad **Ir-L-Os** is well represented by the sum of half the absorption spectra of **Ir-L-Ir** and **Os-L-Os**, thus revealing any significant electronic coupling between the chromophores (Figure S8).

To shed light on the nature of the absorption bands observed in the metalated complexes, DFT and TD-DFT calculations have been performed on **Os-L-Os** and **Ir-L-Os** and on the monometallic complexes **Ir-L** and **Os-L**. The comparison of the electron density plots (Figure S12−S14) evidences that, in the case of **Os-L** and **Ir-L**, one of the two arms preserves the characteristics of **L** alone, while the other one accounts for the presence of the transition metal (TM) group, as in the case of the bimetalated complexes. In the monometallic complexes **Ir-L** and **Os-L** (Figure 1), a strong absorption is calculated at 377 nm ($S_0 \rightarrow S_7$) and 378 nm ($S_0 \rightarrow S_{14}$) corresponding to the characteristic absorption bands of the ligand. This transition is characterized by an excitation completely localized on the alone arm of **L**, while excitations from the other arm contribute to many weaker calculated transitions which occur in the range 365−432 nm. The absorption band which appears at higher

dx.doi.org/10.1021/ic201903g | Inorg. Chem. 2012, 51, 2832−2840

Table 2. Luminescence Properties of Ligand and Complexes[a]

		298 K			77 K		
		λ_{max} (nm)	ϕ	τ (ns)	λ_{max} (nm)	τ (μs)	E (eV)
L	^{1}L	394	0.94	1.1	368, 388	0.89×10^{-3}	3.37
	^{3}L				550, 590, 640(sh)	115.0×10^{3}	2.25
Ir-L	^{1}L	402	2.3×10^{-3}		367, 388		3.38
	^{3}Ir	640	0.031	205.0	546, 594, 642	3.8; 9.5[c]	2.27
Ir-L-Ir	^{1}L	404	ca. 2.0×10^{-3}				
	^{3}Ir	640	0.032	198.0	548, 596, 642	4.7; 11.5[c]	2.26
Os-L	^{1}L	402	3.2×10^{-3}		368, 388		3.37
	^{3}Os	798	1.7×10^{-3}	26.2	738	0.67	1.68
Os-L-Os	^{1}L	406	ca. 3.0×10^{-3}		368, 388		3.37
	^{3}Os	806	1.5×10^{-3}	21.6	750	0.56	1.65
Ir-L-Os	^{1}L	404	ca. 2.0×10^{-2}		369, 390		3.36
	^{3}Ir	640	6.2×10^{-4}	2.4[b]	547, 595, 643	5.2×10^{-3}; 77.4×10^{-3}[b,d]	2.27
	^{3}Os	798	1.7×10^{-3}	24.5	740	0.61	1.68

[a]In air-free solvents, CH_2Cl_2 for the ligand and CH_3CN for the complexes, from corrected spectra. λ_{exc} = 320, 390, and 490 nm for quantum yield determination and 331, 373, and 465 nm for lifetime measurements (see text). [b]Upon excitation at 373 nm. [c]Ratio ca. 30:70. [d]Ratio ca. 50:50.

wavelengths as a shoulder of the intense absorption at 361 nm (Figure 1) in both complexes, is originated by transitions characterized by excitations, which start from both arms of **L** and end onto the metalated part of the complex, widely spreading over TM and its connected **L** arm. The excitations from the TM group also contribute to the description of the transitions occurring in this range of wavelengths and largely characterize absorptions at higher wavelengths.

In the case of bimetallic spiro-compounds the electronic distribution of both arms of **L** is modified by the bond with the TM groups to such an extent that the characteristic absorption of **L** alone is no more observed in the spectra of the complexes (Figure 2). In fact, two nearly degenerate fairly intense transitions are calculated at about 375 nm ($S_0 \rightarrow S_{33}$ and $S_0 \rightarrow S_{34}$) for **Os-L-Os**. They are characterized by electronic excitations arising from **L** and ending on the **Os** terminal groups and assigned to the feature observed at 371 nm in Figure 2. Thus excitations starting from **L** mainly characterize the "anomalous" spectral features in the range around 371 nm, though they mostly combine with transitions predominantly localized on **Os**. We can assume a similar interpretation for the spectral shape of the absorption spectrum of **Ir-L-Ir** in the same region. In the case of the **Os-L-Ir** complex, the calculated transitions in the range 371−430 nm assign the absorption band to excitations to lower states (from $S_0 \rightarrow S_7$ to $S_0 \rightarrow S_{24}$) than those calculated for **Os-L-Os** (from $S_0 \rightarrow S_{21}$ to $S_0 \rightarrow S_{34}$). This is due to the fact that the electrons localized at **L** are relatively more stable in the Os rather than in the Ir complexes of this family. On the whole the effect of linking a TM group to **L** is that of lowering both the transition energies and the relative intensities of excitations, which are originated by this fragment of the complex.

Emission. On the basis of the absorption data, the metallic units and the spiro-bifluorene core could be considered as weakly interacting chromophores in the analysis of the luminescence properties of the systems and separately addressed. Selective excitation of the Os metal center in the Os-containing arrays can be achieved at wavelengths longer than 460 nm (Figures 1 and 2). The prevalent excitation of the Ir metal center in the monometallic complex **Ir-L** and in dyad **Ir-L-Ir** can be pursued at 390 nm. In the case of triad **Ir-L-Os**, excitation at 390 nm populates both Ir and Os based excited states in a 1:1 ratio (Figures 1 and 2 and Table S2−S3). A prevalent excitation of the ligand is difficult to achieve, particularly in the bimetallic complexes, but at 320 nm a small peak corresponding to a $\pi-\pi^*$ transition of the ligand is present in all the complexes (Figures 1 and 2).

Selective excitation of the Os fragment in the Os-containing complexes yielded in all cases similar emission maxima, quantum yields, and lifetimes (Table 2 and Figure S9), which can be attributed to ^{3}MLCT phosphorescence.[50] Only **Os-L-Os** differentiates to some extent showing a red-shifted emission with a shorter lifetime and a lower quantum yield (see Table 2).

Ir-L and **Ir-L-Ir**, upon excitation at 390 nm, present a moderately intense emission centered at ca. 640 nm, with a quantum yield of 0.030 and a lifetime of 200 ns in deaerated solution (Table 2). Although the spectra are bathochromically shifted with respect to that of the parent complex $[Ir(C\hat{}N)_2(bpy)]^+$ (λ_{max} = 590 nm), the emission quantum yields and lifetimes are comparatively higher (ϕ = 0.018 and τ = 180 ns for the latter).[51] This enhancement can be attributed to the delocalization on the bpy ancillary ligand brought by the ethynyl-spirofluorene framework, as shown by the electron density plot (Figure S13). The k_r of the order of 1.5×10^5 s^{-1} is anyway indicative of a ^{3}MLCT emission.[49] The emission spectra of air-free isoabsorbing solutions of **Ir-L**, **Os-L**, and **Ir-L-Os** excited at 390 nm are compared in Figure 3. The residual

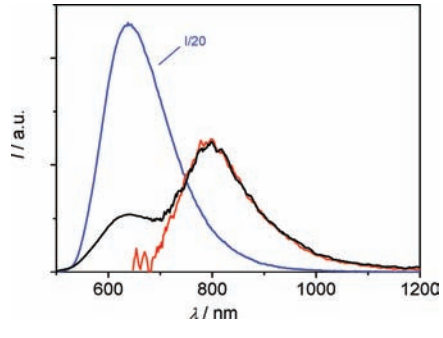

Figure 3. Corrected emission spectra of optically matched air-free CH_3CN solutions of **Ir-L** (blue), **Os-L** (red), and **Ir-L-Os** (black) excited at 390 nm (A_{390}= 0.105). The emission spectrum of **Ir-L** is divided by 20.

dx.doi.org/10.1021/ic201903g | Inorg. Chem. 2012, 51, 2832−2840

Ir based emission observable at 640 nm corresponds to 2% that of model **Ir-L** (Table 2), whereas the Os based emission is completely recovered. The lifetime of the Ir residual emission is 2.4 ns (Table 2) and the luminescence of the Os counterpart at 800 nm, upon excitation at 373 nm, shows a rise time of ca. 2 ns (Figure S10). These data point toward an efficient (η_{EnT} = 0.99; $k_{EnT} = 4.1 \times 10^8$ s^{-1}) energy transfer process from the Ir metal center toward the Os counterpart in triad **Ir-L-Os** (shown as process 3 in Scheme 3).

Scheme 3. Schematic Representation of the Energy Levels of the Excited States of the Examined Complexes (in eV) and of the Photoinduced Energy-Transfer Processes

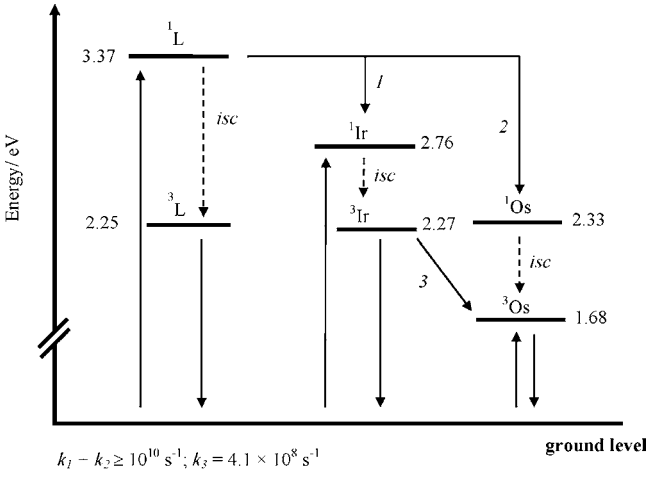

For a Förster-type energy transfer mechanism, a critical radius R_c = 24.0 Å is obtained (Table S4) for the ^{3}Ir → ^{3}Os pathway, corresponding to an efficiency η_{EnT} = 0.5. To account for the observed EnT efficiency an interchromophore separation d = 11.4 Å would be required ($k_F = k_{EnT}$), significantly shorter than that obtained by our molecular modeling of the **Ir-L-Os** array (d_{Ir-Os} = 17.5 Å). On the other hand, for a Dexter-type mechanism, a $J_D = 1.41 \times 10^{-4}$ cm is calculated, yielding a small electronic-coupling term H = 1.57 cm^{-1} for $k_D = k_{EnT}$, typical of through-bond interaction in condensed aromatic systems.[10] Therefore, for the ^{3}Ir→^{3}Os energy transfer step the Dexter-type mechanism is almost exclusively active over a distance larger than 17 Å. This is possibly due to the presence of the long spiroconjugated bridge, that allows an efficient electronic coupling between the donor and acceptor components via an indirect superexchange process mediated by the virtual orbitals (VOs) of the bridging ligand,[52] as also confirmed by the DFT calculated stabilization energies of the examined complexes.

Ligand **L** displays a strong fluorescence (ϕ = 0.94) centered at 394 nm with a lifetime of 1.1 ns (Table 2). To study the photoinduced processes that can occur upon population of the ligand-centered singlet excited state, that lies at energy higher than both Ir and Os metal centered levels (Table 2), the emission spectra of all the mononuclear and binuclear complexes upon excitation at 320 nm have been examined. Figure 4 shows the emission spectra of optically matched solutions of **L**, **Ir-L**, **Ir-L-Ir**, **Os-L**, **Os-L-Os**, and **Ir-L-Os** excited at 320. It emerges that the fluorescence of the ligand is strongly quenched in all monometallic and bimetallic arrays. In **Ir-L**, **Ir-L-Ir**, **Os-L**, and **Os-L-Os**, in fact, a residual emission that accounts for only 0.2−0.3% that of the free ligand can be

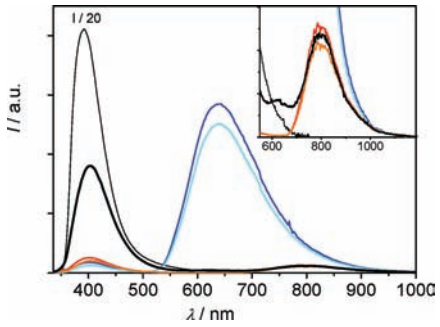

Figure 4. Corrected emission spectra of air-free solutions of **L** (black thin) in CH_2Cl_2 and of **Ir-L** (blue), **Ir-L-Ir** (cyan), **Os-L** (red), **Os-L-Os** (orange), and **Ir-L-Os** (black thick) in CH_3CN excited at 320 nm (A_{320} = 0.110). The spectrum of **L** is divided by 20. The range 550−1200 nm is expanded in the inset.

observed, while in triad **Ir-L-Os** a somewhat minor quenching of the ligand fluorescence can be envisaged (residual emission of about 2% that of the ligand, Figure 4). Although it is not possible to exclude that part of the detected fluorescence derives from traces (<0.1%) of the free ligand in the samples of the complexes, we can safely assign the observed luminescence mainly to the residual ligand fluorescence inside the complexes, in particular for the **Ir-L-Os** case. The rate constants for the ligand-based fluorescence quenching are thus on the order of 10^{10} s^{-1} for **Ir-L-Os** and $\geq 10^{12}$ s^{-1} for the other complexes. One can assume that the recovery of the Ir-based emission at 640 nm in **Ir-L** and **Ir-L-Ir** and of the Os emission at 800 nm in **Os-L** and **Os-L-Os**, upon excitation of the ligand, is almost complete. Notably, upon excitation of the ligand singlet in triad **Ir-L-Os**, the Ir-centered emission is almost absent (a small peak at 620 nm with an estimated intensity of about 5% that of **Ir-L** can be detected, inset of Figure 4), whereas the Os emission is quite completely recovered with respect to that of **Os-L** and **Os-L-Os** (Figure 4). A direct ^{1}L→^{1}Os energy transfer process can thus be envisaged as the predominant path for **L** deactivation in **Ir-L-Os** (pathway 2 in Scheme 3), followed by intersystem crossing to ^{3}Os, in a way similar to that observed in a truxene-based system.[10,11] The ^{1}L→^{1}Ir energy transfer (pathway 1 in Scheme 3), followed by intersystem crossing and terminating with the ^{3}Ir→^{3}Os transfer, instead seems to be disfavored. A plausible explanation is the favorable large energy gap between the singlet levels of ligand and Os. A further support is given by the theoretical calculations that evidenced the dominant contribution of the Os-polypyridyl group with respect to the Ir counterpart in the frontier orbitals of the triad (Figure S14 and Table S3).

A similar scenario is observed at 77 K in glassy matrix. In fact, upon excitation at 390 nm, the quenching of the Ir based emission in the triad **Ir-L-Os**, and the quite complete recovery of the Os centered emission has been observed (Figure 5). The ligand excitation at 320 nm produces the complete sensitization of the Ir and Os emissions in the monometallic dyads, and almost full recovery of the Os-based phosphorescence in **Ir-L-Os** (Figure 6).[53] Interestingly, ligand phosphorescence has been observed at 77 K upon addition of methylene iodide to the solution (Figure S11). The triplet state, with a lifetime of 115 ms, is located at 2.25 eV and is thus almost isoenergetic with the Ir-centered triplet of the complexes, which at low temperature is localized at 2.27 eV (Table 2). The L→Ir energy transfer path at low temperature could thus proceed also via population of the ligand triplet, induced by the presence of the

dx.doi.org/10.1021/ic201903g | Inorg. Chem. 2012, 51, 2832−2840

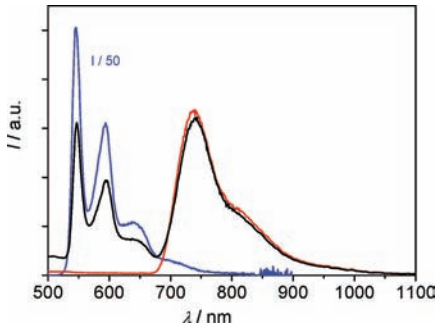

Figure 5. Corrected emission spectra at 77 K of optically matched MeOH/EtOH 1:4 (1:4 v/v) solutions of **Ir-L** (blue), **Os-L** (red), and **Ir-L-Os** (black) excited at 390 nm (A_{390}= 0.093). The emission spectrum of **Ir-L** is divided by 50.

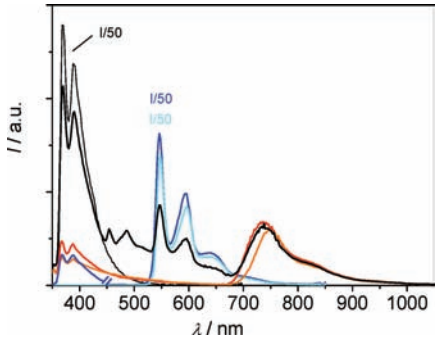

Figure 6. Corrected emission spectra at 77 K of optically matched MeOH/EtOH (1:4 v/v) solutions of **L** (black thin), **Ir-L** (blue), **Ir-L-Ir** (cyan), **Os-L** (red), **Os-L-Os** (orange), and **Ir-L-Os** (black thick) excited at 320 nm (A_{320}= 0.100). The emission spectra of **L**, **Ir-L**, and **Ir-L-Ir** are divided by 50.

heavy Ir and Os atoms. The data point, however, to a prevalent L→Os direct energy transfer, similarly to that observed at room temperature, with a concomitant transfer of the energy directly absorbed by the Ir unit toward the Os ^{3}MLCT state (Scheme 3).

CONCLUSIONS

In summary, we have synthesized and investigated the photophysical properties of new Ir, Os, and mixed Ir/Os spirobifluorene-based complexes and of the bis-bipyridine spirobifluorene ligand. The absorption features of the monometallic and bimetallic arrays in the 300−450 nm region have been interpreted on the basis of TD-DFT calculations, which evidenced mixed ligand and metal based transitions. Besides, the coincidence of the absorption spectrum of the target heterobimetallic derivative with the linear combination of half of the absorption spectra of the homobimetallic analogues indicated negligible interactions in the ground state between the metallic units, enabling a photophysical study on the basis of the individual electronic properties of the components.

The spirobifluorene unit behaves as an active partner in the photophysics of the arrays and not as a mere structural motif, due to its remarkable luminescence properties. An energy transfer cascade starting from the ligand singlet has been envisaged in all the examined arrays. The ligand fluorescence is, in fact, almost quantitatively quenched in all the mono- and bimetallic systems at both temperatures and efficient energy transfer toward the appended metal chromophores is operative. The Ir-based luminescence, observed in model compounds **Ir-L** and **Ir-L-Ir**, is strongly quenched in the **Ir-L-Os** complex. Interestingly, the Ir→Os energy transfer, which occurs with k_{EnT} = 4.1 × 10^8 s^{-1}, is well described by a Dexter type mechanism that involves the ligand orbitals, characterized by the particular spiroconjugation. In the target heterometallic triad, thus, excitation of both the spiro ligand or the Ir center quantitatively generates the phosphorescent ^{3}Os state. Low-temperature measurements evidenced that the ligand triplet is close-lying with the Ir emissive triplet, whereas the population of the former in the triad seems to be disfavored in favor of the more exothermic L→Os deactivation path.

In conclusion, the data show that the spirobifluorene framework can be successfully employed for the construction of antenna arrays with an orthogonal displacement in space of the chromophores, opening the way to newly conceived optoelectronic devices.

ASSOCIATED CONTENT

Supporting Information

Traces of thin-layer chromatography (Figure S1); traces of the proton-NMR spectra (Figures S2−S7); additional photophysical data (Figures S8−S11); details on theoretical calculations (pages S8−S9); electron density plots and S_0→S_n calculated transitions of **L**, **Os-L**, **Ir-L**, **Os-L-Os**, and **Ir-L-Os** (Figures S12−S14 and Tables S1−S3); parameters for evaluation of energy-transfer mechanisms (Table S4). This material is available free of charge via the Internet at http://pubs.acs.org.

AUTHOR INFORMATION

Corresponding Author

*E-mail: bventura@isof.cnr.it (B.V.); ziessel@unistra.fr (R.Z.).

Notes

The authors declare no competing financial interest.

ACKNOWLEDGMENTS

Funding from CNR of Italy (Projects PM.P04.010 MACOL and ESF-EUROCORES SolarFuelTandem), MIUR (Projects FIRB-RBIP0642YL LUCI and NODIS), and the Centre National de la Recherche Scientifique (CNRS in France) are acknowledged. We warmly thank Thomas Bura from the LCOSA laboratory for preparing the NMR traces for all samples.

REFERENCES

(1) Balzani, V.; Bergamini, G.; Ceroni, P. *Coord. Chem. Rev.* **2008**, *252*, 2456−2469.
(2) Balzani, V.; Credi, A.; Venturi, M. *Molecular Devices and Machines: Concepts and Perspectives for the Nanoworld*, 2nd ed.; Wiley: Weinheim, 2008.
(3) Muro, M. L.; Rachford, A. A.; Wang, X. H.; Castellano, F. N. *Top. Organomet. Chem.* **2010**, *29*, 159−191.
(4) Rausch, A. F.; Homeier, H. H. H.; Yersin, H. *Top. Organomet. Chem.* **2010**, *29*, 193−235.
(5) Harriman, A.; Ziessel, R. *Chem. Commun.* **1996**, 1707−1716.
(6) Serin, J. M.; Brousmiche, D. W.; Frechet, J. M. J. *Chem. Commun.* **2002**, 2605−2607.
(7) Williams, J. A. G. *Top. Curr. Chem.* **2007**, *281*, 205−268.
(8) Cotlet, M.; Vosch, T.; Habuchi, S.; Weil, T.; Mullen, K.; Hofkens, J.; De Schryver, F. *J. Am. Chem. Soc.* **2005**, *127*, 9760−9768.
(9) Diring, S.; Puntoriero, F.; Nastasi, F.; Campagna, S.; Ziessel, R. *J. Am. Chem. Soc.* **2009**, *131*, 6108−6110.
(10) Diring, S.; Ziessel, R.; Barigelletti, F.; Barbieri, A.; Ventura, B. *Chem.—Eur. J.* **2010**, *16*, 9226−9236.

(11) Ventura, B.; Barbieri, A.; Barigelletti, F.; Diring, S.; Ziessel, R. *Inorg. Chem.* **2010**, *49*, 8333−8346.
(12) Simmons, H. E.; Fukunaga, T. *J. Am. Chem. Soc.* **1967**, 5208−5215.
(13) Sagiv, J.; Yogev, A.; M., Y. *J. Am. Chem. Soc.* **1977**, *99*, 6861−6869.
(14) Palmieri, P.; Samori, B. *J. Am. Chem. Soc.* **1981**, *103*, 6818−6823.
(15) Bendazzoli, G.; Degli Esposti, A.; Palmieri, P.; Marconi, G.; Samori, B. *J. Chem. Soc., Faraday Trans.* **1982**, *78*, 1623−1631.
(16) Gleiter, R.; Schafer, W. *Acc. Chem. Res.* **1990**, *23*, 369−375.
(17) Rizzo, F.; Cavazzini, M.; Righetto, S.; De Angelis, F.; Fantacci, S.; Quici, S. *Eur. J. Org. Chem.* **2010**, 4004−4016.
(18) Cao, X. Y.; Zhang, W.; Zi, H.; Pei, J. *Org. Lett.* **2004**, *6*, 4845−4848.
(19) Jahng, Y.; Rahman, A. *Bull. Chem. Soc. Jpn.* **2010**, *83*, 672−677.
(20) Saragi, T. P. I; Spehr, T.; Siebert, A.; Fuhrmann-Lieker, T.; Salbeck, J. *Chem. Rev.* **2007**, *107*, 1011−1065.
(21) Katsis, D.; Geng, Y. H.; Ou, J. J.; Culligan, S. W.; Trajkovska, A.; Chen, S. H.; Rothberg, L. J. *Chem. Mater.* **2002**, *14*, 1332−1339.
(22) Park, J. H.; Ko, H. C.; Kim, J. H.; Lee, H. *Synth. Met.* **2004**, *144*, 193−199.
(23) Tseng, Y. H.; Shih, P. I.; Chien, C. H.; Dixit, A. K.; Shu, C. F.; Liu, Y. H.; Lee, G. H. *Macromolecules* **2005**, *38*, 10055−10060.
(24) Vak, D.; Shin, S. J.; Yum, J. H.; Kim, S. S.; Kim, D. Y. *J. Lumin.* **2005**, *115*, 109−116.
(25) Yang, Z. D.; Feng, J. K.; Ren, A. M. *Chem. Phys. Lett.* **2008**, *461*, 9−15.
(26) Heredia, D.; Natera, J.; Gervaldo, M.; Otero, L.; Fungo, F.; Lin, C. Y.; Wong, K. T. *Org. Lett.* **2010**, *12*, 12−15.
(27) Kowada, T.; Yamaguchi, S.; Ohe, K. *Org. Lett.* **2010**, *12*, 296−299.
(28) Montalti, M.; Credi, A.; Prodi, L.; Gandolfi, M. T. *Handbook of Photochemistry*, 3rd ed.; CRC Press, Taylor & Francis: Boca Raton, FL, 2006.
(29) Sauvage, J. P.; Collin, J. P.; Chambron, J. C.; Guillerez, S.; Coudret, C.; Balzani, V.; Barigelletti, F.; Decola, L.; Flamigni, L. *Chem. Rev.* **1994**, *94*, 993−1019.
(30) Demas, J. N.; Crosby, G. A. *J. Phys. Chem.* **1971**, *75*, 991−1024.
(31) Barigelletti, F.; Flamigni, L. *Chem. Soc. Rev.* **2000**, *29*, 1−12.
(32) Sessler, J. L.; Jayawickramarajah, J.; Sathiosatham, M., Energy and Electron Transfer in Supramolecular Systems. In *Encyclopedia of Supramolecular Chemistry*; Atwood, J. L., Steed, J. W., Eds.; CRC Press: Boca Raton, FL, 2004; Vol. *1*, pp 535−545.
(33) Hohenberg, P.; Kohn, W. *Phys. Rev.* **1964**, *136*, B864−B871.
(34) Kohn, W.; Sham, L. J. *Phys. Rev.* **1965**, *140*, A1133−A1138.
(35) Bauernschmitt, R.; Ahlrichs, R. *Chem. Phys. Lett.* **1996**, *256*, 454−464.
(36) Casida, M. E.; Jamorski, C.; Casida, K. C.; Salahub, D. R. *J. Chem. Phys.* **1998**, *108*, 4439−4449.
(37) Stratmann, R. E.; Scuseria, G. E.; Frisch, M. J. *J. Chem. Phys.* **1998**, *109*, 8218−8224.
(38) Frisch, M. J., et al. *Gaussian 09, Revision A.2*; Gaussian, Inc.: Wallingford, CT, 2009.
(39) Zhao, Y.; Truhlar, D. G. *Theor. Chem. Acc.* **2008**, *120*, 215−241.
(40) Figgen, D.; Peterson, K. A.; Dolg, M.; Stoll, H. *J. Chem. Phys.* **2009**, *130*, 164108.
(41) Hariharan, P.; Pople, J. *Theor. Chem. Acc.* **1973**, *28*, 213−222.
(42) Hehre, W. J.; Ditchfield, R.; Pople, J. A. J. *J. Chem. Phys.* **1972**, *56*, 2257−2261.
(43) Tomasi, J.; Mennucci, B.; Cammi, R. *Chem. Rev.* **2005**, *105*, 2999−3093.
(44) Foster, P.; Weinhold, F. *J. Am. Chem. Soc.* **1980**, *102*, 7211−7218.
(45) Grosshenny, V.; Romero, F. M.; Ziessel, R. *J. Org. Chem.* **1997**, *62*, 1491−1500.
(46) Thiemann, F.; Piehler, T.; Haase, D.; Saak, W.; Lutzen, A. *Eur. J. Org. Chem.* **2005**, 1991−2001.
(47) Buckingham, D. A.; Dwyer, F. P.; Goodwin, H. A.; Sargeson, A. M. *Aust. J. Chem.* **1964**, *17*, 325−336.
(48) Sajoto, T.; Djurovich, P. I.; Tamayo, A. B.; Oxgaard, J.; Goddard, W. A.; Thompson, M. E. *J. Am. Chem. Soc.* **2009**, *131*, 9813−9822.
(49) Flamigni, L.; Barbieri, A.; Sabatini, C.; Ventura, B.; Barigelletti, F. Photochemistry and photophysics of coordination compounds: Iridium. In *Photochemistry and Photophysics of Coordination Compounds II*; Balzani, V., Campagna, S., Eds.; Springer-Verlag: Berlin, 2007; Vol. *281*, pp 143−203.
(50) Kumaresan, D.; Shankar, K.; Vaidya, S.; Schmehl, R. H., Photochemistry and photophysics of coordination compounds: Osmium. In *Photochemistry and Photophysics of Coordination Compounds II*; Balzani, V., Campagna, S., Eds.; Springer-Verlag: Berlin, 2007; Vol. *281*, pp 101−142.
(51) Glusac, K. D.; Jiang, S. J.; Schanze, K. S. *Chem. Commun.* **2002**, 2504−2505.
(52) Chiorboli, C.; Indelli, M. T.; Scandola, F. In *Molecular Wires and Electronics*; De Cola, L., Ed.; Springer: Berlin, 2005; Vol. *257*, pp 63−102.
(53) It can be noticed that whereas for **Ir-L**, **Os-L**, **Os-L-Os**, **Ir-L-Os** the two characteristic peaks of the ligand fluorescence are well distinguishable at 368 and 388 nm, in dyad **Ir-L-Ir** no fluorescence at all in the range 350−450 nm could be detected.